

## Disket-Nanorings of $K_2Ti_6O_{13}$ Formed by Self-Spiraling of a Nanobelt

Cheng-Yan Xu,<sup>†,‡,§</sup> Yu-Zi Liu,<sup>†,§</sup> Liang Zhen,<sup>‡</sup> and Zhong Lin Wang\*,<sup>†</sup>

School of Materials Science and Engineering, Georgia Institute of Technology, Atlanta, Georgia 30332, and School of Materials Science and Engineering, Harbin Institute of Technology, Harbin 150001, China

Received: March 12, 2008; Revised Manuscript Received: April 1, 2008

Single-crystal  $K_2Ti_6O_{13}$  nanorings were prepared by molten salt synthesis. The nanoring is formed by loop-by-loop winding of a  $K_2Ti_6O_{13}$  nanobelt by coherently matching the lattice at the edges of the nanobelt in the same plane. The driving force for such a perfect match at the edges is suggested to minimize the local electrostatic energy introduced by the cations and anions.

### Introduction

Free-standing nanorings, as a new nanostructure for some oxides, have attracted intense interest since their first discovery in piezoelectric  $ZnO$ .<sup>1</sup> The wurtzite structure of  $ZnO$  produces positively charged (0001)-Zn and negatively charged (0001)-O polar surfaces, resulting in a normal dipole moment and spontaneous polarization. Minimizing the electrostatic interaction energy is the driving force for the self-coiling process of a polar nanobelt to form a “single-crystal” nanoring as well as their various derivations such as nanohelixes and nanosprings.<sup>2</sup> The spontaneous polarization-induced growth process was also applied for the interpretation of the formation of other wurtzite-structured nanorings, such as AlN nanorings,<sup>3</sup> GaN nanorings,<sup>4</sup> and also other nonwurtzite-structured nanorings, for example,  $CuO$ <sup>5</sup> and  $Ag_2V_4O_{11}$ <sup>6</sup> with monoclinic structure and  $Ba_{1+x^-}V_{6}O_{16} \cdot nH_2O$  with hewettite structure.<sup>7</sup> As to the synthesis routes, the reported approaches to the preparation of self-coiled, free-standing nanorings were limited to solid–vapor or solution phase processes. No report on the solid-state synthesis of free-standing nanorings could be found.

In this paper, we report the first discovery of  $K_2Ti_6O_{13}$  disket-nanorings formed by self-spiraling of a  $K_2Ti_6O_{13}$  nanobelt, which was prepared by molten salt synthesis (MSS). The structure of the nanoring has been characterized, and the nanoring is formed by loop-by-loop winding of a  $K_2Ti_6O_{13}$  nanobelt by coherently matching the lattice at the edges of the nanobelt in the same plane. The driving force for such a perfect match at the edges is suggested to minimize the local electrostatic energy introduced by the cations and anions.

### Experimental Section

**Synthesis.** Single-crystalline  $K_2Ti_6O_{13}$  nanorings were prepared by molten salt synthesis method, which is similar to our previous report on the synthesis of other alkali titanate and niobate nanowires/nanoribbons.<sup>8</sup> First, 0.046 g of  $K_2C_2O_4$  (Aldrich), 0.04 g of  $TiO_2$  (anatase, Aldrich) nanoparticles,<sup>9</sup> and

2.0 g of KCl were mixed with ~5 mL of Tetrogi NP-9 (Aldrich) and ground for 10 min. Then, the mixture was placed in a combustion boat and annealed in a tube furnace at 800 °C for 3 h and subsequently cooled naturally to room temperature. The resulted powders were washed with distilled water several times to remove remaining KCl and  $K_2C_2O_4$ .

**Characterization.** X-ray diffraction (XRD) patterns were collected using a Philips X'pert diffractometer with high-intensity Cu  $K\alpha$  irradiation ( $\lambda = 1.5406 \text{ \AA}$ ). Morphology of the nanorings was characterized by scanning electron microscope (SEM, LEO 1530). High-resolution transmission electron microscope (HRTEM) observations were carried out on a JEOL 4000EX microscope at accelerating voltage of 400 kV. Energy-dispersive X-ray spectroscopy (EDS) analysis was conducted by using a Hitachi HF2000 microscope. Crystal structure mode of  $K_2Ti_6O_{13}$  was built by using MSI CERIUS<sup>2</sup> software.

### Results and Discussion

Figure 1a shows an overview of the as-synthesized product, which consists of a wealth of nanobelts, platelets as well as many free-standing nanorings. The rings have typical diameters of ~1 to 5  $\mu\text{m}$  and wall thickness of several hundreds nanometers. High-magnification SEM image (Figure 1b) clearly showed a perfect circular shape of the complete ring. XRD revealed that the as-synthesized product including the nanorings is a single phase  $K_2Ti_6O_{13}$  (Figure 1c) with lattice parameters  $a = 15.59$ ,  $b = 3.796$ ,  $c = 9.108 \text{ \AA}$ , and  $\beta = 99.78^\circ$  (JCPDS 40–0403). Through the magnified SEM images presented in Figures 1b,d, the nanoring is clearly a result of winding nanowire/nanobelts around its circumferences loop by loop. The nonuniform contrast indicates the variation in the morphology in the disket surface.

HRTEM was used for further study of the microstructure and morphology of the nanorings. Figures 2a,b display a representative bright-field TEM image and corresponding dark-field image of a nanoring at low magnification. The nonuniform contrast in around the nanoring indicates the presence of strain and lattice distortion. The chemical composition of a nanoring is best determined by EDS in TEM, which was acquired at 200 kV using a Hitachi HF2000 microscope, as shown in the inset in Figure 2a, clearly showing the presence of the desired elements

\* To whom correspondence should be addressed. Fax: 1-404-894-8008. Phone: 1-404-894-8008. E-mail: zhong.wang@mse.gatech.edu.

† Georgia Institute of Technology.

‡ Harbin Institute of Technology.

§ Both authors contributed equally to this paper.

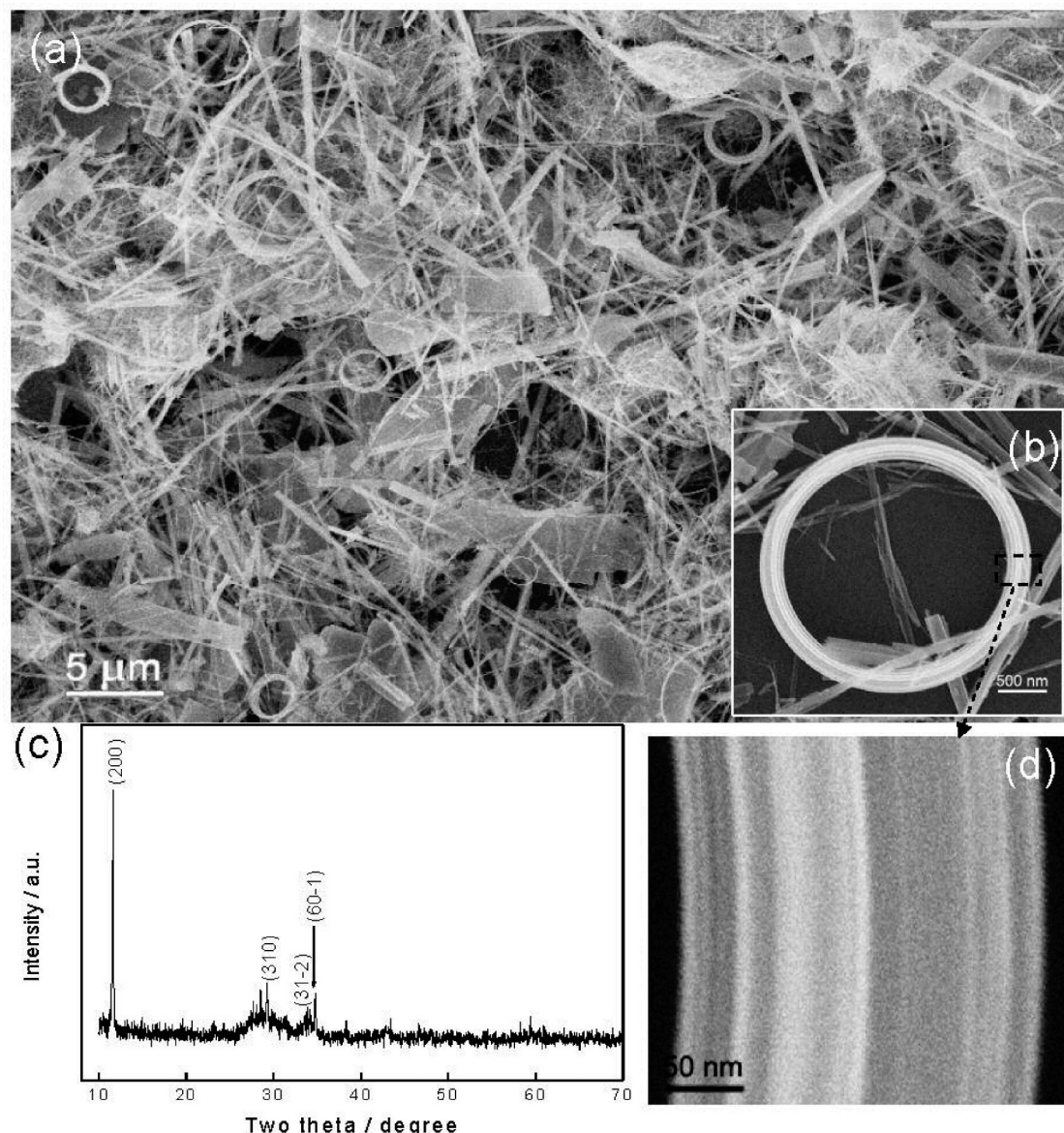


**Figure 1.** (a) SEM image of the as-received synthesized product. (b) A free-standing  $\text{K}_2\text{Ti}_6\text{O}_{13}$  nanoring. (c) XRD pattern received from the sample to confirm the crystal structure. (d) An enlarged SEM image of a segment of the nanoring shown in panel b, displaying the looping morphology of the nanoring.

in the sample. Selected-area electron diffraction patterns taken from different parts of the nanoring and labeled c, d, and e, are given in Figure 1 panels c, d, and e, respectively. The diffraction patterns are identical except that they rotate following the local tangential orientation of the nanoring. The ring apparently has a “single-crystal” structure. Indexing of the electron diffraction shows that the normal direction of the disket ring is [001]; the nanobelt that forms the ring has a growth front plane of (010) and side surfaces (100). The nanoring is formed by spiraling the nanobelt by matching the (200) sides surfaces. The growth direction of the nanobelt is in agreement with previously reported  $\text{K}_2\text{Ti}_6\text{O}_{13}$  nanowires.<sup>10</sup>

The loop-by-loop self-spiraling of the nanobelt is directly depicted by high-magnification TEM image along the ring, as shown in Figure 3a, where the radial contrast is apparent and the width of the nanobelt remains fairly constant during the spiraling. The number of loops of this nanobelt is  $\sim 65$ . By carefully examining the most inner loop and most outer loop, we did find the starting end (Figure 3b) and finishing end (Figure 3c) of the nanobelt of width  $\sim 6$  nm. This is solid evidence that

shows that the disket nanoring was made by loop-by-loop winding of a nanobelt in the ring plane.

The spiraling of  $\text{K}_2\text{Ti}_6\text{O}_{13}$  nanorings is different from that of previously reported  $\text{ZnO}$  nanorings, of which the spiraling follows the “slinky” spring and usually introduces a small helical angle.<sup>1</sup> As to the  $\text{K}_2\text{Ti}_6\text{O}_{13}$  nanorings, the spiraling of nanobelt is the in-plane spiraling.

The detailed structure at the interface between the two consecutive loops of the spiraling nanobelt has been revealed by high-resolution TEM. As guided by the low-magnification TEM image, we were able to track the location of the interface. Shown in Figure 3d is a HRTEM image that shows the lattice image of several periods of the spiraling nanobelts. The image clearly shows the single crystal structure, although the possible waving contrast introduced by the “buckling” can be identified. By selecting a region as indicated by a rectangle around an interface between the two consecutive loops, the details of the interface is presented in Figure 3e. Using the standard crystal structure model of  $\text{K}_2\text{Ti}_6\text{O}_{13}$  and following the orientation relationship as provided by the electron diffraction, the [001]

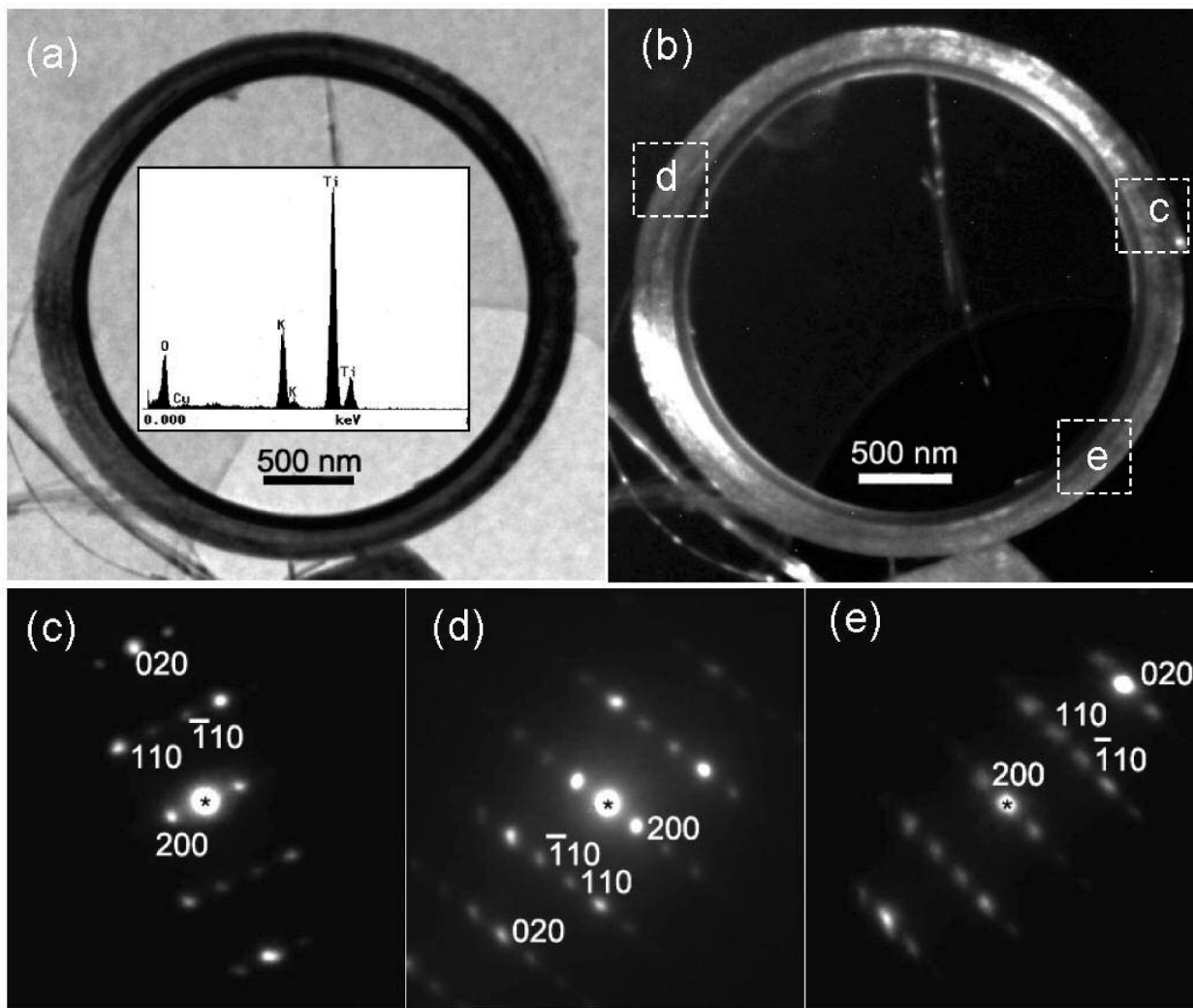


**Figure 2.** (a) Bright-field and (b) dark-field TEM images of a  $\text{K}_2\text{Ti}_6\text{O}_{13}$  nanoring. (c–e) Corresponding electron diffraction patterns recorded from the c, d, and e areas labeled in panel b. The spiraling direction is [010] and the outer edge surface of the nanoring is (200).

orientation simulated HRTEM image is inset in the image. The simulated HRTEM of  $\text{K}_2\text{Ti}_6\text{O}_{13}$  with a 20 period unit cells in *c* axis was performed using MSI CERIUS<sup>2</sup> software with system default JEOL 4000EX microscope under defocus of 143.88 nm. By comparing the simulated image with the experimental observed one, the interface shows a “perfect” coherent match without stacking faults, which means that the consecutive loops of the nanobelts form a perfect lattice and there is no interface.

To understand the formation of the coherent interface and the driving force for forcing the nanobelt to spiraling, we now examine the atomic structure of the nanobelt. Monoclinic  $\text{K}_2\text{Ti}_6\text{O}_{13}$  has a tunnel structure, which is formed by connecting corners of opposing octahedra from adjacent layers composed by edge-sharing  $\text{TiO}_6$  octahedrons (see Figure 4a). Potassium ions are situated in the rectangle tunnels. When the nanobelt grows along [010], its top and bottom surfaces are  $\pm(001)$ , and the two side surfaces are  $\pm(100)$ , which requires the cleavage of two adjacent layers, and thus the closed frameworks embedding potassium ions are separated ones at each side surface (Figure 4a). The K atoms appear in pairs, but they are displaced with respect to each other along the *c*-axes (Figure 4b). In such a case, the local surface is made of alternative distribution of  $\text{K}^+$  and  $\text{O}^{2-}$  in the form of chess pattern along both *b*- and *c*-axes in the (100) plane (Figure 4d). The  $\text{K}^+$  ion is located in the channel and the  $\text{O}^{2-}$  ions are at the apex of the octahedron.

After the nanobelt runs for a full loop and at the interfacing region, the two side surfaces of the same nanobelt will meet and combine. The most natural way is to match the two interfaces with the  $\text{K}^+$  at one side surface directly facing the  $\text{O}^{2-}$  at the other side surface, which is schematically shown using the chess pattern in Figure 4d. If the surface structure is perfect as we have described in Figure 4a, such a matching as depicted in Figure 4d results in excess  $\text{O}^{2-}$ . In practice, this may not be a problem because oxygen vacancies are frequently observed in oxides and surfaces. Such vacancy sites may be filled in by the excess oxygen after forming the interface, resulting in a stable structure.

In general, the nanobelts tend to be straight if its lateral dimension is larger. However, for the very fine nanobelt of  $\sim 6$  nm in width, it is very flexible with the increase of its length. A long nanobelt may be fold back and by chance the surfaces of the folded nanobelt may meet. Atomic level ionic interaction may align the loops of the nanobelt to form a coherent interface. The radius of the loop may be a result of how the nanobelt folds during its initial growth, but the size of the loop cannot be too small to reduce the elastic deformation energy. Once this first loop is established, the following is a self-spiral as the growth proceeds. The spiraling of the nanobelt introduces local strain and buckling, which is evident in the image shown in Figure 3d.

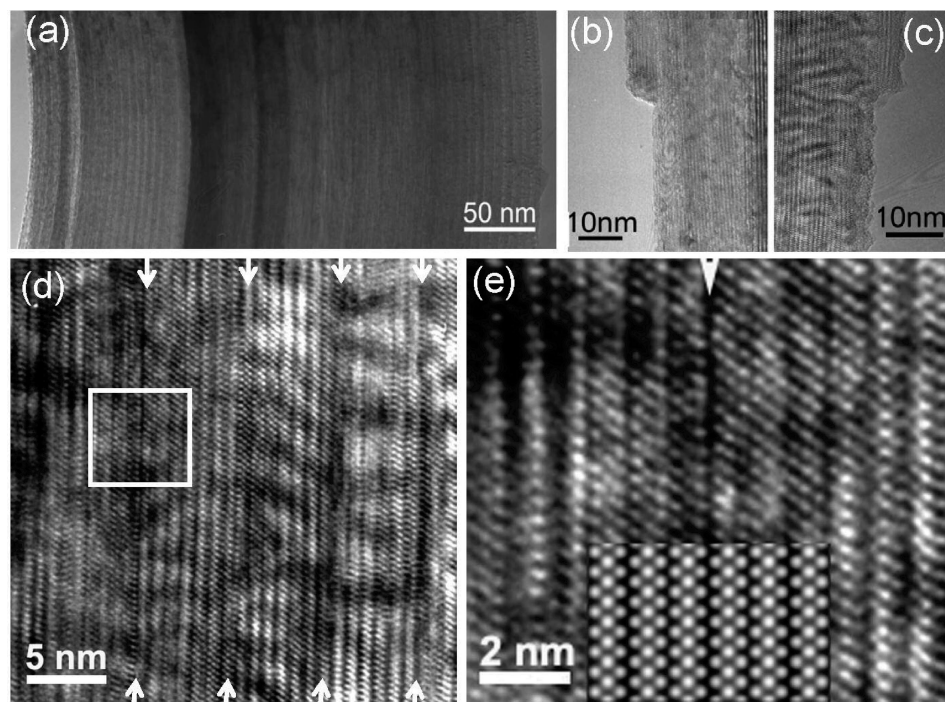


**Figure 3.** (a) High-resolution TEM image of a  $\text{K}_2\text{Ti}_6\text{O}_{13}$  nanoring, showing the loop-by-loop spiral of a nanobelt. (b,c) The starting end and finishing ends of the spiral nanobelt located at the inner and outer edges of the disket-nanoring. (d) HRTEM image of the nanoring in which the interface between the two consecutive loops of the spiraling nanobelt is indicated by arrowheads. (e) An enlarged HRTEM image from the interface region of the interface as indicated by a square box in panel d. The inset at the bottom is a simulated image based on the structure model given in Figure 4a. The simulation was carried out under the following conditions: acceleration voltage  $V = 400.0$  kV, spherical aberration coefficient  $C_s = 0.50$  mm, aperture size  $A_p = 0.80 \text{ \AA}^{-1}$ , defocus spread  $D_{\text{rms}} = 100.0 \text{ \AA}$ , beam divergence 0.5 mrad, vibration 0.35  $\text{\AA}$ , and the sample thickness of 182.24  $\text{\AA}$ .

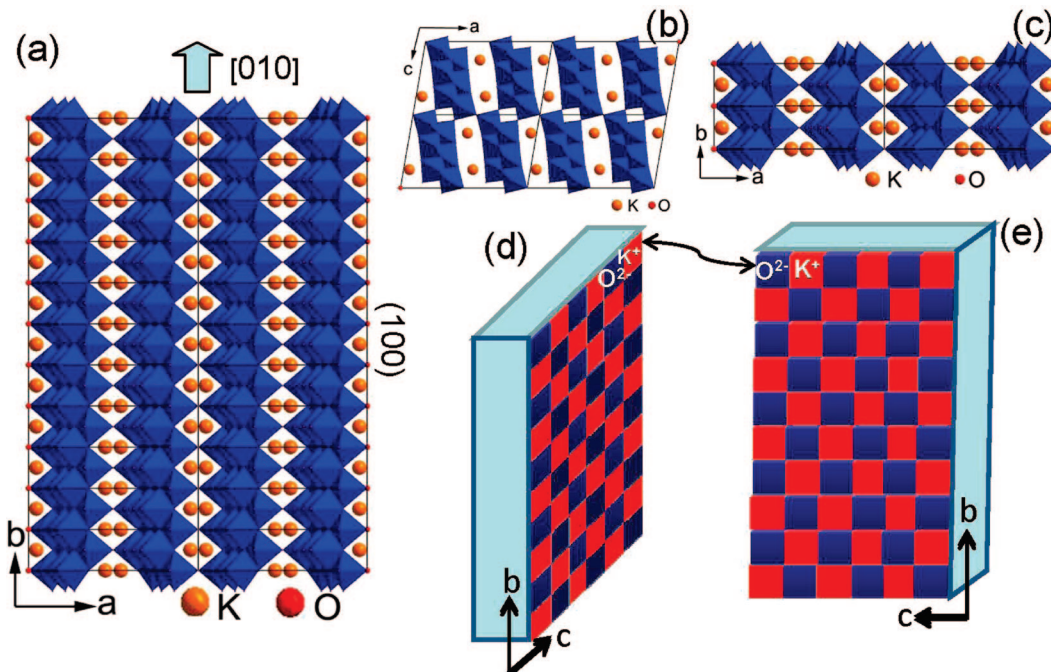


**Figure 4.** (a) Atomic structure of the  $\text{K}_2\text{Ti}_6\text{O}_{13}$  nanobelt with growth direction [010], side surfaces (100), and top and bottom surfaces (001). (b,c) Projection of the unit cell of  $\text{K}_2\text{Ti}_6\text{O}_{13}$  along the  $b$ - and  $c$ -axis, respectively. (d,e) Schematic chess pattern representation of the cation and anion distribution in the (100) plane, parallel to which the two spiral loops meet. The red area corresponds to  $\text{O}^{2-}$ , and the blue area corresponds to  $\text{K}^+$ .

The probability that a nanobelt folds over to form a loop depends on entropy. No ring will be formed if this first step was not initiated. In comparison to the percentage of straight nanobelts in the final synthesis product (Figure 1a), the population of the nanorings is low.

## Conclusions

In summary, we have synthesized  $\text{K}_2\text{Ti}_6\text{O}_{13}$  nanorings via the molten salt approach for the first time. The disket-nanoring of  $\text{K}_2\text{Ti}_6\text{O}_{13}$  is formed by self-spiraling of a nanobelt growing

along its [010] direction by coherently matching the (010) side surfaces, which is suggested to be driven by minimizing the interaction energy of local ionic charges as contributed by K<sup>+</sup> and O<sup>2-</sup>.

**Acknowledgment.** This work was supported by DOE BES (DE-FG02-07ER46394), and NSF (DMS 0706436). C.Y.X. was supported by the Development Program for Outstanding Young Teachers and Internationalization Foundation of HIT.

## References and Notes

- (1) Kong, X. Y.; Ding, Y.; Yang, R.; Wang, Z. L. *Science* **2004**, *303*, 1348.
- (2) (a) Kong, X. Y.; Wang, Z. L. *Nano Lett.* **2003**, *3*, 1625. (b) Kong, X. Y.; Wang, Z. L. *Appl. Phys. Lett.* **2004**, *84*, 975. (c) Hughes, W. L.; Wang, Z. L. *J. Am. Chem. Soc.* **2004**, *126*, 6703.
- (3) Duan, J. H.; Yang, S. G.; Liu, H. W.; Gong, J. F.; Huang, H. B.; Zhao, X. N.; Tang, J. L.; Zhang, Z.; Du, Y. W. *J. Cryst. Growth* **2005**, *283*, 291.
- (4) Jian, J. K.; Zhang, Z. H.; Sun, Y. P.; Lei, M.; Chen, X. L.; Wang, T. M.; Wang, C. *J. Cryst. Growth* **2007**, *303*, 427.
- (5) Wang, X. Q.; Xi, G. C.; Xiong, S. L.; Liu, Y. K.; Xi, B. J.; Yu, W. C.; Qian, Y. T. *Cryst. Growth Des.* **2007**, *7*, 930.
- (6) Shen, G. Z.; Chen, D. *J. Am. Chem. Soc.* **2006**, *128*, 11672.
- (7) Pang, S. P.; Li, G. C.; Wang, L.; Zhang, Z. K. *J. Cryst. Growth* **2006**, *293*, 423.
- (8) (a) Xu, C. Y.; Zhang, Q.; Zhang, H.; Zhen, L.; Tang, J.; Qin, L.-C. *J. Am. Chem. Soc.* **2005**, *127*, 11584. (b) Xu, C. Y.; Zhen, L.; Yang, L.; He, K.; Shao, W. Z.; Qin, L.-C. *Ceram. Int.* **2008**, *34*, 435. (c) Xu, C. Y.; Zhen, L.; Yang, R.; Wang, Z.; L. *J. Am. Chem. Soc.* **2007**, *129*, 15444.
- (9) Excess potassium oxalate is necessary for the formation of phase-pure K<sub>2</sub>TiO<sub>3</sub> nanorings. When the molar ratio of K<sub>2</sub>C<sub>2</sub>O<sub>4</sub> to TiO<sub>2</sub> was 1:6, no nanoring was formed.
- (10) (a) Du, G. H.; Chen, Q.; Han, P. D.; Yu, Y.; Peng, L.-M. *Phys. Rev. B* **2003**, *67*, 035323. (b) Wang, R. H.; Chen, Q.; Wang, B. L.; Zhang, S.; Peng, L.-M. *Appl. Phys. Lett.* **2005**, *86*, 133101.  
JP802152K